Development of Numerical Algorithms for Practical Computation of Nonlinear Normal Modes

M. Peeters, F. Georgiades, R. Viguié, G. Sérandour, G. Kerschen, J.C. Golinval
Structural Dynamics Research Group,
Aerospace and Mechanical Engineering Department,
University of Liège, Liège, Belgium
e-mail: **m.peeters,f.georgiades,r.viguie,g.serandour,g.kerschen,jc.golinval@ulg.ac.be**

Abstract

When resorting to numerical algorithms, we show that nonlinear normal mode (NNM) computation is possible with limited implementation effort, which paves the way to a practical method for determining the NNMs of nonlinear mechanical systems. The proposed method relies on two main techniques, namely a shooting procedure and a method for the continuation of NNM motions. In addition, sensitivity analysis is used to reduce the computational burden of the algorithm. A simplified discrete model of a nonlinear bladed disk is considered to demonstrate the developments.

1 Introduction

Nonlinear normal modes (NNMs) offer a solid theoretical and mathematical tool for interpreting a wide class of nonlinear dynamical phenomena, yet they have a clear and simple conceptual relation to the LNMs [1, 2, 3]. However, most structural engineers still view NNMs as a concept that is foreign to them, and they do not yet consider NNMs as a useful concept for structural dynamics. One reason supporting this statement is that most existing constructive techniques for computing NNMs are based on asymptotic approaches and rely on fairly involved mathematical developments.

There have been very few attempts to compute NNMs using numerical methods [4, 5, 6, 7]. Algorithms for the continuation of periodic solutions are really quite sophisticated and advanced (see, e.g., [8, 9, 10]), and they have been extensively used for computing the forced response and limit cycles of nonlinear dynamical systems (see, e.g., [11]). Interestingly, they have not been fully exploited for the computation of nonlinear modes.

The objective of this paper is to support that these numerical algorithms pave the way for an effective and practical computation of NNMs. In the present paper, we show that the NNM computation is possible with limited implementation effort. The proposed algorithm, implemented in MATLAB, relies on two main techniques, namely a shooting procedure and a method for the continuation of NNM motions. The algorithm is demonstrated using a simplified discrete model of a nonlinear bladed disk.

2 Nonlinear Normal Modes (NNMs)

A detailed description of NNMs and their fundamental properties (e.g., frequency-energy dependence, bifurcations and stability) is given in [1, 2, 3]. For completeness, the two main definitions of an NNM are briefly reviewed in this section.

The free response of discrete conservative mechanical systems with n degrees of freedom (DOFs) is considered, assuming that continuous systems (e.g., beams, shells or plates) have been spatially discretized using the finite element method. The equations of motion are

$$\mathbf{M}\,\ddot{\mathbf{x}}(t) + \mathbf{K}\,\mathbf{x}(t) + \mathbf{f}_{\text{nl}}\left\{\mathbf{x}(t), \dot{\mathbf{x}}(t)\right\} = 0 \tag{1}$$

where $\mathbf{M}$ is the mass matrix; $\mathbf{K}$ is the stiffness matrix; $\mathbf{x}$, $\dot{\mathbf{x}}$ and $\ddot{\mathbf{x}}$ are the displacement, velocity and acceleration vectors, respectively; $\mathbf{f}_{\text{nl}}$ is the nonlinear restoring force vector.

There exist two main definitions of an NNM in the literature due to Rosenberg and Shaw and Pierre:

1. Targeting a straightforward nonlinear extension of the linear normal mode (LNM) concept, Rosenberg defined an NNM motion as a *vibration in unison* of the system (i.e., a synchronous periodic oscillation).

2. To provide an extension of the NNM concept to damped systems, Shaw and Pierre defined an NNM as a two-dimensional invariant manifold in phase space. Such a manifold is invariant under the flow (i.e., orbits that start out in the manifold remain in it for all time), which generalizes the invariance property of LNMs to nonlinear systems.

At first glance, Rosenberg's definition may appear restrictive in two cases. Firstly, it cannot be easily extended to nonconservative systems. However, the damped dynamics can often be interpreted based on the topological structure of the NNMs of the underlying conservative system [3]. Secondly, in the presence of internal resonances, the NNM motion is no longer synchronous, but it is still periodic.

In the present study, an NNM motion is therefore defined as a *(non-necessarily synchronous) periodic motion* of the conservative mechanical system (1). As we will show, this extended definition is particularly attractive when targeting a numerical computation of the NNMs. It enables the nonlinear modes to be effectively computed using algorithms for the continuation of periodic solutions.

3 Numerical Computation of NNMs

The numerical method proposed here for the NNM computation relies on two main techniques, namely a shooting technique and the pseudo-arclength continuation method. A detailed description of the algorithm is given in [12].

3.1 Shooting Method

The equations of motion of system (1) can be recast into state space form

$$\dot{\mathbf{z}} = \mathbf{g}(\mathbf{z}) \tag{2}$$

where $\mathbf{z} = [\mathbf{x}^* \quad \dot{\mathbf{x}}^*]^*$ is the $2n$-dimensional state vector, and star denotes the transpose operation, and

$$\mathbf{g}(\mathbf{z}) = \begin{pmatrix} \dot{\mathbf{x}} \\ -\mathbf{M}^{-1}\left[\mathbf{K}\mathbf{x} + \mathbf{f}_{\text{nl}}(\mathbf{x}, \dot{\mathbf{x}})\right] \end{pmatrix} \tag{3}$$

is the vector field. The solution of this dynamical system for initial conditions $\mathbf{z}(0) = \mathbf{z}_0 = [\mathbf{x}_0^* \quad \dot{\mathbf{x}}_0^*]^*$ is written as $\mathbf{z}(t) = \mathbf{z}\left(t, \mathbf{z}_0\right)$ in order to exhibit the dependence on the initial conditions, $\mathbf{z}\left(0, \mathbf{z}_0\right) = \mathbf{z}_0$. A solution $\mathbf{z}_p(t, \mathbf{z}_{p0})$ is a periodic solution of the autonomous system (2) if $\mathbf{z}_p(t, \mathbf{z}_{p0}) = \mathbf{z}_p(t + T, \mathbf{z}_{p0})$, where T is the minimal period.

The NNM computation is carried out by finding the periodic solutions of the governing nonlinear equations of motion (2). In this context, the *shooting method* is probably the most popular numerical technique. It solves numerically the two-point boundary-value problem defined by the periodicity condition

$$\mathbf{H}(\mathbf{z}_{p0}, T) \equiv \mathbf{z}_p(T, \mathbf{z}_{p0}) - \mathbf{z}_{p0} = \mathbf{0} \tag{4}$$

$\mathbf{H}(\mathbf{z}_0, T) = \mathbf{z}(T, \mathbf{z}_0) - \mathbf{z}_0$ is called the *shooting function* and represents the difference between the initial conditions and the system response at time T. Unlike forced motion, the period T of the free response is not known a priori.

The shooting method consists in finding, in an iterative way, the initial conditions $\mathbf{z}_{p0}$ and the period T that realize a periodic motion. To this end, the method relies on direct numerical time integration and on the Newton-Raphson algorithm.

Starting from some assumed initial conditions $\mathbf{z}_{p0}^{(0)}$, the motion $\mathbf{z}_p^{(0)}(t, \mathbf{z}_{p0}^{(0)})$ at the assumed period $T^{(0)}$ can be obtained by numerical time integration methods (e.g., Runge-Kutta or Newmark schemes). In general, the initial guess $(\mathbf{z}_{p0}^{(0)}, T^{(0)})$ does not satisfy the periodicity condition (4). A Newton-Raphson iteration scheme is therefore to be used to correct an initial guess and to converge to the actual solution. The corrections $\Delta\mathbf{z}_{p0}^{(k)}$ and $\Delta T^{(k)}$ at iteration k are found by expanding the nonlinear function

$$\mathbf{H}\left(\mathbf{z}_{p0}^{(k)} + \Delta\mathbf{z}_{p0}^{(k)}, T^{(k)} + \Delta T^{(k)}\right) = 0 \tag{5}$$

in Taylor series and neglecting higher-order terms (H.O.T.).

The phase of the periodic solutions is not fixed. If $\mathbf{z}(t)$ is a solution of the autonomous system (2), then $\mathbf{z}(t + \Delta t)$ is geometrically the same solution in state space for any Δt. Hence, an additional condition, termed the *phase condition*, has to be specified in order to remove the arbitrariness of the initial conditions. This is discussed in detail in [12].

In summary, an isolated NNM is computed by solving the augmented two-point boundary-value problem defined by

$$\mathbf{F}(\mathbf{z}_{p0}, T) \equiv \left\{ \begin{array}{rcl} \mathbf{H}(\mathbf{z}_{p0}, T) & = & 0 \\ h(\mathbf{z}_{p0}) & = & 0 \end{array} \right. \tag{6}$$

where $h(\mathbf{z}_{p0}) = 0$ is the phase condition.

3.2 Continuation of Periodic Solutions

Due to the frequency-energy dependence, the modal parameters of an NNM vary with the total energy. An NNM family, governed by equations (6), therefore traces a curve, termed an NNM branch, in the $(2n + 1)$-dimensional space of initial conditions and period $(\mathbf{z}_{p0}, T)$. Starting from the corresponding LNM at low energy, the computation is carried out by finding successive points $(\mathbf{z}_{p0}, T)$ of the NNM branch using methods for the *numerical continuation* of periodic motions (also called *path-following methods*) [8, 9]. The space $(\mathbf{z}_{p0}, T)$ is termed the continuation space.

Different methods for numerical continuation have been proposed in the literature. The so-called pseudo-arclength continuation method is used herein.

Starting from a known solution $(\mathbf{z}_{p0,(j)}, T_{(j)})$, the next periodic solution $(\mathbf{z}_{p0,(j+1)}, T_{(j+1)})$ on the branch is computed using a *predictor step* and a *corrector step*.

Predictor step

At step j, a prediction $(\tilde{\mathbf{z}}_{p0,(j+1)}, \tilde{T}_{(j+1)})$ of the next solution $(\mathbf{z}_{p0,(j+1)}, T_{(j+1)})$ is generated along the tangent vector to the branch at the current point $\mathbf{z}_{p0,(j)}$

$$\begin{bmatrix} \tilde{\mathbf{z}}_{p0,(j+1)} \\ \tilde{T}_{(j+1)} \end{bmatrix} = \begin{bmatrix} \mathbf{z}_{p0,(j)} \\ T_{(j)} \end{bmatrix} + s_{(j)} \begin{bmatrix} \mathbf{p}_{z,(j)} \\ p_{T,(j)} \end{bmatrix} \tag{7}$$

where $s_{(j)}$ is the predictor stepsize. The tangent vector $\mathbf{p}_{(j)} = [\mathbf{p}^*_{z,(j)}\ p_{T,(j)}]^*$ to the branch defined by (6) is solution of the system

$$\begin{bmatrix} \frac{\partial \mathbf{H}}{\partial \mathbf{z}_{p0}}\Big|_{(\mathbf{z}_{p0,(j)}, T_{(j)})} & \frac{\partial \mathbf{H}}{\partial T}\Big|_{(\mathbf{z}_{p0,(j)}, T_{(j)})} \\ \frac{\partial h}{\partial \mathbf{z}_{p0}}^*\Big|_{(\mathbf{z}_{p0,(j)})} & 0 \end{bmatrix} \begin{bmatrix} \mathbf{p}_{z,(j)} \\ p_{T,(j)} \end{bmatrix} = \begin{bmatrix} \mathbf{0} \\ 0 \end{bmatrix} \tag{8}$$

with the condition $\left\|\mathbf{p}_{(j)}\right\| = 1$. The star denotes the transpose operator. This normalization can be taken into account by fixing one component of the tangent vector and solving the resulting overdetermined system using the Moore-Penrose matrix inverse; the tangent vector is then normalized to 1.

Corrector step

The prediction is corrected by a shooting procedure in order to solve (6) in which the variations of the initial conditions and the period are forced to be orthogonal to the predictor step. At iteration k, the corrections

$$\begin{aligned} \mathbf{z}^{(k+1)}_{p0,(j+1)} &= \mathbf{z}^{(k)}_{p0,(j+1)} + \Delta\mathbf{z}^{(k)}_{p0,(j+1)} \\ T^{(k+1)}_{(j+1)} &= T^{(k)}_{(j+1)} + \Delta T^{(k)}_{(j+1)} \end{aligned} \tag{9}$$

are computed by solving the overdetermined linear system using the Moore-Penrose matrix inverse

$$\begin{bmatrix} \frac{\partial \mathbf{H}}{\partial \mathbf{z}_{p0}}\Big|_{(\mathbf{z}^{(k)}_{p0,(j+1)}, T^{(k)}_{(j+1)})} & \frac{\partial \mathbf{H}}{\partial T}\Big|_{(\mathbf{z}^{(k)}_{p0,(j+1)}, T^{(k)}_{(j+1)})} \\ \frac{\partial h}{\partial \mathbf{z}_{p0}}^*\Big|_{(\mathbf{z}^{(k)}_{p0,(j+1)})} & 0 \\ \mathbf{p}^*_{z,(j)} & p_{T,(j)} \end{bmatrix} \begin{bmatrix} \Delta\mathbf{z}^{(k)}_{p0,(j+1)} \\ \Delta T^{(k)}_{(j+1)} \end{bmatrix} = \begin{bmatrix} -\mathbf{H}(\mathbf{z}^{(k)}_{p0,(j+1)}, T^{(k)}_{(j+1)}) \\ -h(\mathbf{z}^{(k)}_{p0,(j+1)}) \\ 0 \end{bmatrix} \tag{10}$$

where the prediction is used as initial guess, i.e, $\mathbf{z}^{(0)}_{p0,(j+1)} = \tilde{\mathbf{z}}_{p0,(j+1)}$ and $T^{(0)}_{(j+1)} = \tilde{T}_{(j+1)}$. The last equation in (10) corresponds to the orthogonality condition for the corrector step.

This iterative process is carried out until convergence is achieved. The convergence test is based on the relative error of the periodicity condition:

$$\frac{\|\mathbf{H}(\mathbf{z}_{p0}, T)\|}{\|\mathbf{z}_{p0}\|} = \frac{\|\mathbf{z}_p(T, \mathbf{z}_{p0}) - \mathbf{z}_{p0}\|}{\|\mathbf{z}_{p0}\|} < \epsilon \tag{11}$$

where ϵ is the prescribed relative precision.

3.3 Sensitivity Analysis

Each shooting iteration involves the time integration of the equations of motion to evaluate the current shooting residue $\mathbf{H}\left(\mathbf{z}^{(k)}_{p0}, T^{(k)}\right) = \mathbf{z}^{(k)}_p(T^{(k)}, \mathbf{z}^{(k)}_{p0}) - \mathbf{z}^{(k)}_{p0}$. As evidenced by equation (10), the method also requires the evaluation of the $2n \times 2n$ Jacobian matrix

$$\frac{\partial \mathbf{H}}{\partial \mathbf{z}_0}(\mathbf{z}_0, T) = \left.\frac{\partial \mathbf{z}(t, \mathbf{z}_0)}{\partial \mathbf{z}_0}\right|_{t=T} - \mathbf{I} \tag{12}$$

where $\mathbf{I}$ is the $2n \times 2n$ identity matrix.

The classical finite-difference approach requires to perturb successively each of the $2n$ initial conditions and integrate the *nonlinear* governing equations of motion. This approximate method therefore relies on extensive numerical simulations and may be computationally intensive for large-scale finite element models.

Targeting a reduction of the computational cost, a significant improvement is to use sensitivity analysis for determining $\partial \mathbf{z}(t, \mathbf{z}_0)/\partial \mathbf{z}_0$ instead of a numerical finite-difference procedure. The sensitivity analysis consists in differentiating the equations of motion (2) with respect to the initial conditions $\mathbf{z}_0$ which leads to

$$\frac{d}{dt}\left[\frac{\partial \mathbf{z}\,(t, \mathbf{z}_0)}{\partial \mathbf{z}_0}\right] = \left.\frac{\partial \mathbf{g}(\mathbf{z})}{\partial \mathbf{z}}\right|_{\mathbf{z}(t,\mathbf{z}_0)} \left[\frac{\partial \mathbf{z}(t, \mathbf{z}_0)}{\partial \mathbf{z}_0}\right] \tag{13}$$

with

$$\frac{\partial \mathbf{z}(0, \mathbf{z}_0)}{\partial \mathbf{z}_0} = \mathbf{I} \tag{14}$$

since $\mathbf{z}(0, \mathbf{z}_0) = \mathbf{z}_0$. Hence, the matrix $\partial \mathbf{z}(t, \mathbf{z}_0)/\partial \mathbf{z}_0$ at $t = T$ can be obtained by numerically integrating over T the initial-value problem defined by the *linear* ordinary differential equations (ODEs) (13) with the initial conditions (14).

In addition to the integration of the current solution $\mathbf{z}(t, \mathbf{x}_0)$ of (2), these two methods for computing $\partial \mathbf{z}(t, \mathbf{z}_0)/\partial \mathbf{z}_0$ require $2n$ numerical integrations of $2n$-dimensional dynamical systems, which may be computationally intensive for large systems. However, equations (13) are linear ODEs and their numerical integration is thus less expensive. The numerical cost can be further reduced if the solution of equations (13) is computed together with the solution of the nonlinear equations of motion in a single numerical simulation [13].

The sensitivity analysis requires only one additional iteration at each time step of the numerical time integration of the current motion to provide the Jacobian matrix. The reduction of the computational cost is therefore significant for large-scale finite element models. In addition, the Jacobian computation by means of the sensitivity analysis is exact. The convergence troubles regarding the chosen perturbations of the finite-difference method are then avoided. Hence, the use of sensitivity analysis to perform the shooting procedure represents a meaningful improvement from a computational point of view.

As the monodromy matrix $\partial \mathbf{z}_p(T, \mathbf{z}_{p0})/\partial \mathbf{z}_{p0}$ is computed, its eigenvalues, the Floquet multipliers, are obtained as a by-product, and the stability analysis of the NNM motions can be performed in a straightforward manner.

3.4 Algorithm for NNM Computation

The algorithm proposed for the computation of NNM motions is a combination of shooting and pseudo-arclength continuation methods, as shown in Figure 1. It has been implemented in the MATLAB environment. Other features of the algorithm such as the step control, the reduction of the computational burden and the method used for numerical integration of the equations of motion are discussed in [12].

So far, the NNMs have been considered as branches in the continuation space $(\mathbf{z}_{p0}, T)$. An appropriate graphical depiction of the NNMs is to represent them in a frequency-energy plot (FEP). This FEP can be computed in a straightforward manner: (i) the conserved total energy is computed from the initial conditions realizing the NNM motion; and (ii) the frequency of the NNM motion is calculated directly from the period.

4 Numerical Experiment - Nonlinear Bladed Disk System

The NNM computation method is now demonstrated using a simplified mathematical model of a nonlinear bladed disk assembly. The lumped parameter model admits a single degree of freedom for each blade and

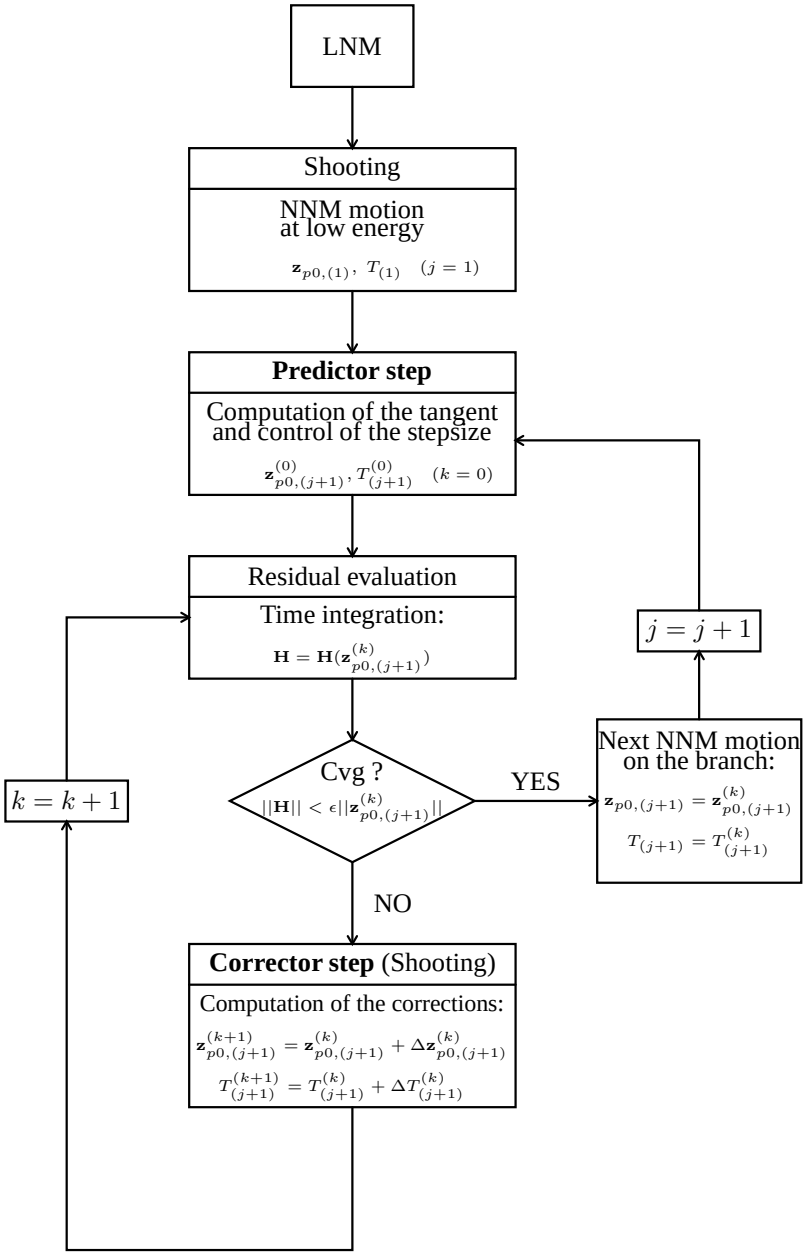

Figure 1: Algorithm for NNM computation.

includes a similarly simplified representation of the flexible disk. The bladed disk is composed of 30 sectors assembled with cyclic periodicity; a single sector is represented in Figure 2. Each sector is modeled using disk (M) and blade (m) lumped masses, coupled by linear (k) and cubic (k_{nl}) springs. The nonlinear springs can, for instance, be representative of geometrically nonlinear effects in slender blades. The disk masses are connected together by linear springs K. The equations of motion of this 60-DOF system are

$$\begin{aligned} m\,\ddot{x}_i + k(x_i - X_i) + k_{nl}(x_i - X_i)^3 &= 0 \\ M\,\ddot{X}_i + K(X_i - X_{i+1}) + K(X_i - X_{i-1}) + k(X_i - x_i) + k_{nl}(X_i - x_i)^3 &= 0 \end{aligned} \tag{15}$$

for $i = 1, \ldots, 30$; $X_{31} = X_1$, $X_0 = X_{30}$ (conditions of cyclic periodicity). X_i and x_i are the displacements of the disk and blade masses of the ith sector, respectively. The values $M = 1$, $m = 0.3$, $K = 1$, $k = 1$, $k_{nl} = 0.1$ are used in this study.

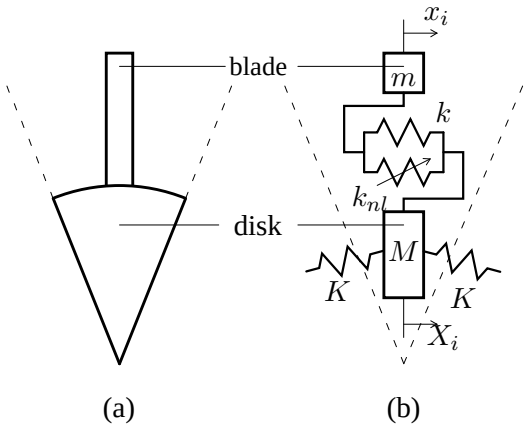

Figure 2: One sector of the nonlinear bladed disk assembly. (a) continuous structure; (b) discrete model.

Mode	Nodal circles	Nodal diameters	Freq. (rad/s)	Mode	Nodal circles	Nodal diameters	Freq. (rad/s)
1	0	0	0.000	31	1	0	2.082
2,3	0	1	0.183	32,33	1	1	2.084
4,5	0	2	0.363	34,35	1	2	2.092
6,7	0	3	0.536	36,37	1	3	2.104
8,9	0	4	0.700	38,39	1	4	2.123
10,11	0	5	0.850	40,41	1	5	2.147
12,13	0	6	0.985	42,43	1	6	2.178
14,15	0	7	1.103	44,45	1	7	2.215
16,17	0	8	1.202	46,47	1	8	2.258
18,19	0	9	1.282	48,49	1	9	2.304
20,21	0	10	1.346	50,51	1	10	2.350
22,23	0	11	1.394	52,53	1	11	2.394
24,25	0	12	1.428	54,55	1	12	2.431
26,27	0	13	1.452	56,57	1	13	2.460
28,29	0	14	1.465	58,59	1	14	2.478
30	0	15	1.470	60	1	15	2.485

Table 1: Natural frequencies of the underlying linear bladed assembly.

4.1 Modal Analysis of the Underlying Linear System

Before studying the nonlinear bladed disk assembly, the natural frequencies and mode shapes of the underlying linear system are first discussed. All bladed assemblies with circumferential symmetry exhibit certain well-defined types of vibration mode [14]. A key feature is the existence of two types of mode, *single* and *double*:

- The modes that occur in pair represent the majority. They have the same natural frequency and similar mode shapes. In fact, no unique mode shapes can be specified for these modes. Rather, it is sufficient to specify two suitably orthogonal shapes and to note that, when vibrating freely at that natural frequency, the structure can assume any form given by a linear combination of the two specified shapes. The mode shape is characterized by n *nodal diameters* since the displacement is constrained to be zero along n-equally spaced diametral lines. The mode shapes of a mode pair have mutually orthogonal nodal diameters.
- The assembly also possesses a smaller number of single modes. They correspond to motion with all

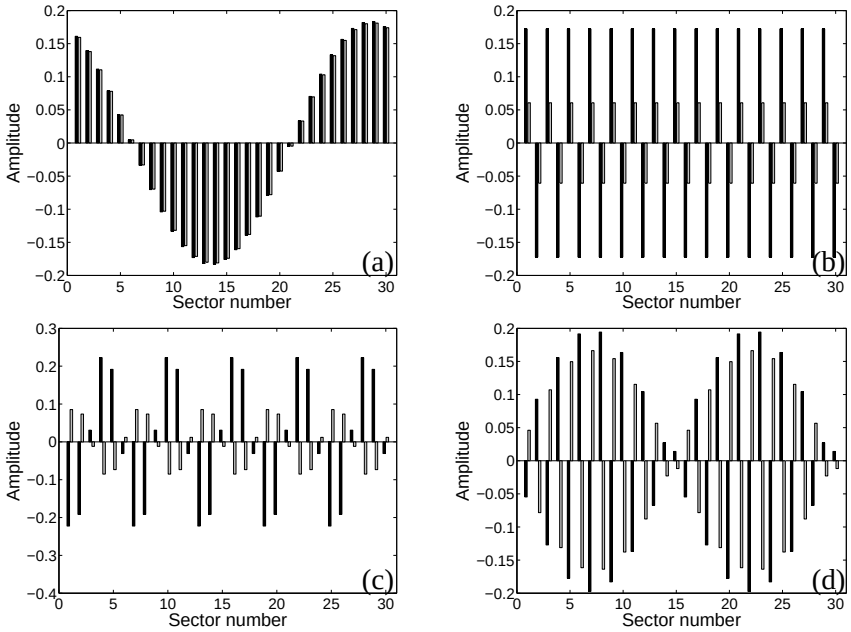

Figure 3: Representative LNMs of the bladed assembly; the blade and disk masses are shown in black and grey, respectively. One mode of the mode pair (a) (0,1); (b) (0,15); (c) (1,5) and (d) (1,14).

the blades having the same amplitude of motion, either in phase with each other (0 nodal diameter) or out of phase with their neighbors (N/2 nodal diameters).

The natural frequencies of the underlying linear bladed assembly are listed in Table 1. In this table, the modes are denoted by the integer pair (n,m), which corresponds to the number of nodal circles and nodal diameters for the considered mode, respectively. In the model (15), the nodal circle parameter n can only take the values $n = 0$ or $n = 1$, according to whether the blade and disk masses undergo in-phase or out-of-phase motion, respectively. One observes the existence of 28 pairs of double modes and 4 single modes. Figure 3 depicts four representative LNMs of the bladed assembly, namely mode (0,15) and one mode of the mode pairs (0,1), (1,5) and (1,14).

4.2 Nonlinear Normal Modes (NNMs)

Modal analysis of the nonlinear bladed assembly is carried out in this section using the previously described algorithm. Starting from the corresponding LNMs at low energy and gradually increasing the total energy in the system, NNM branches are computed. These branches, termed backbone branches, are represented in Figure 4 and form the skeleton of the FEP. As we shall see, other NNM branches bifurcate from and coalesce into these backbone branches.

The first noticeable feature in Figure 4 is the frequency-energy dependence of the NNMs. The oscillation frequency of the modes with 1 nodal circle is strongly affected by the nonlinearities in the system. For these modes, the blade and disk masses vibrate in an out-of-phase fashion, which enhances nonlinear effects. On the other hand, the oscillation frequency of the modes with 0 nodal circle is much less affected. This is because the blade and disk masses vibrate in an in-phase fashion for these modes.

4.2.1 Similar and Nonsimilar NNMs

In addition to the dependence of their oscillation frequency, the NNMs may also have their modal shapes that vary with the total energy in the system. According to Rosenberg's terminology [15], a similar NNM corre-

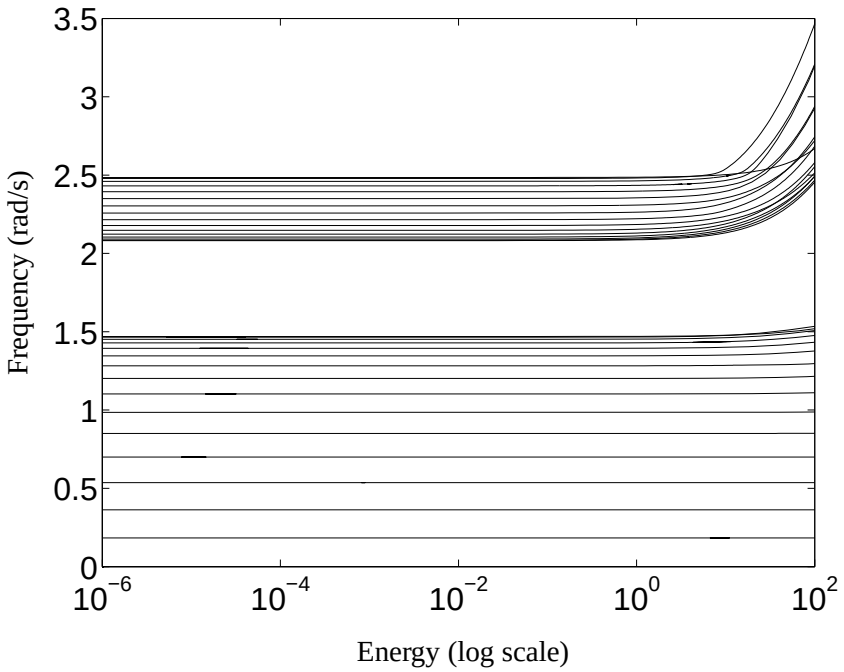

Figure 4: Evolution of the NNM frequencies with the total energy in the system.

sponds to an (energy-independent) straight modal line in the configuration space and occurs only in systems presenting certain spatial symmetries. A nonsimilar NNM corresponds to a curve in the configuration space, the shape of which varies with the total energy. Due to its symmetry properties, the system possesses both similar and nonsimilar NNMs. Two examples of similar NNMs in the bladed disk are the nonlinear extension of the LNMs with 0 nodal diameters, namely modes (0,0) and (1,0). Mode (0,0) is a rigid-body mode, which is obviously unaffected by nonlinearity. The FEP of mode (1,0) in Figure 5 clearly depicts that, while the NNM frequency is altered by the nonlinearities in the system, the modal shape remains unchanged.

Nonsimilar NNMs resemble the corresponding LNMs at low energy. The structure (i.e., the number of nodal circles and diameters) is preserved, and, as for the modes of the linear system, they mostly appear in pair. Nonsimilar NNMs in this system are either weakly, moderately or strongly affected by nonlinearity for increasing energy levels:

- Figure 6 represents a mode of the mode pair (0,2), whose shape is almost energy-independent.
- Figure 7 shows that the NNM motions of mode pair (0,14) have a marked energy dependence.
- A remarkable property of the NNM motions of mode (1,14) is that the vibrational energy localizes to a limited number of sectors, the remaining of the system being virtually motionless (see Figure 8). The resulting spatial confinement of the energy causes the responses of some blades to become dangerously high and might lead to premature high cycle fatigue of the blades. For illustration, the time series corresponding to such an NNM motion are displayed in Figure 9. This localization phenomenon was also observed in linear mistuned bladed assemblies [16], but, here, it occurs even in the absence of structural disorder. It results from the frequency-energy dependence inherent to nonlinear oscillations and is discussed in detail in references [17, 18, 19].

4.2.2 Modal Interaction: Internally Resonant NNMs

When carrying out the NNM computation at higher energies, other resonance scenarios can be observed through the occurrence of tongues of internally resonant NNMs. Unlike backbone branches, tongues are localized to a specific region of the FEP. They bifurcate from a backbone branch of a specific mode and

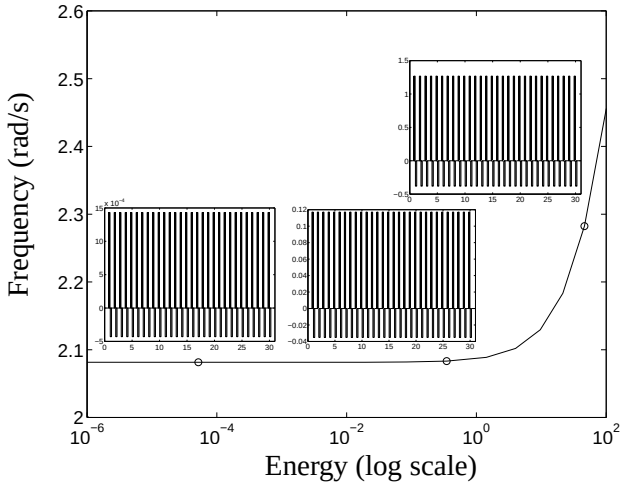

Figure 5: FEP of mode (1,0). NNM represented by bar graphs are inset; they are given in terms of the initial displacements that realize the periodic motion (with zero initial velocities assumed). The blade and disk masses are shown in black and grey, respectively.

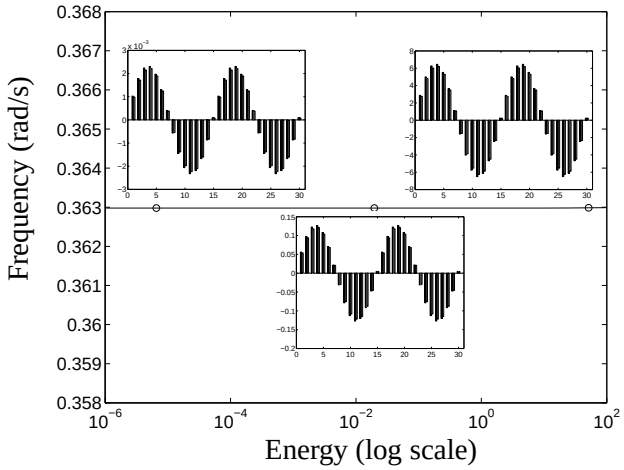

Figure 6: FEP of one mode of the mode pair (0,2). NNM represented by bar graphs are inset; they are given in terms of the initial displacements that realize the periodic motion (with zero initial velocities assumed). The blade and disk masses are shown in black and grey, respectively.

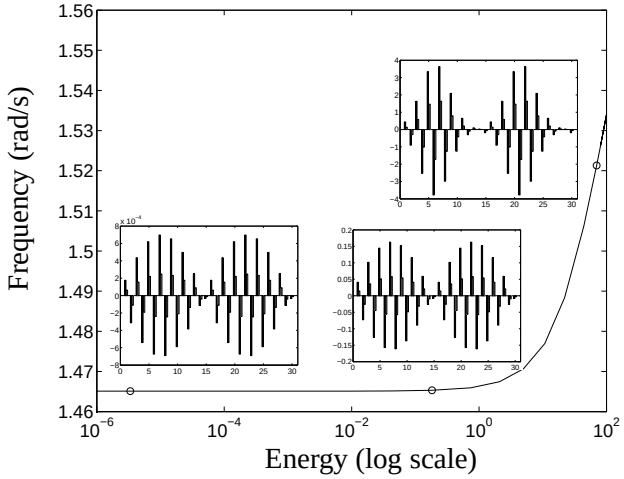

Figure 7: FEP of one mode of the mode pair (0,14). NNM represented by bar graphs are inset; they are given in terms of the initial displacements that realize the periodic motion (with zero initial velocities assumed). The blade and disk masses are shown in black and grey, respectively.

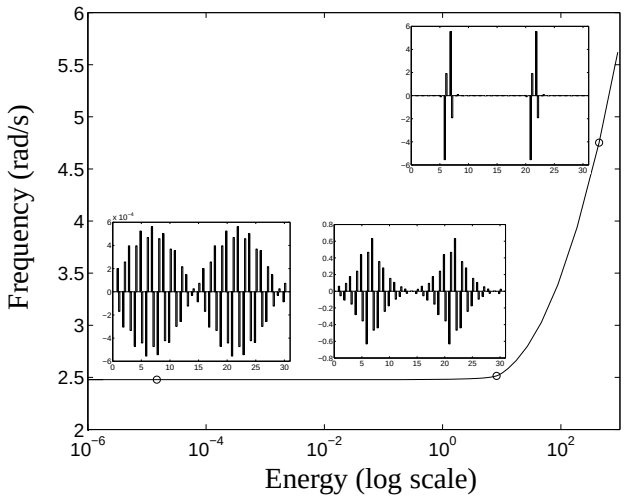

Figure 8: FEP of one mode of the mode pair (1,14). NNM represented by bar graphs are inset; they are given in terms of the initial displacements that realize the periodic motion (with zero initial velocities assumed). The blade and disk masses are shown in black and grey, respectively.

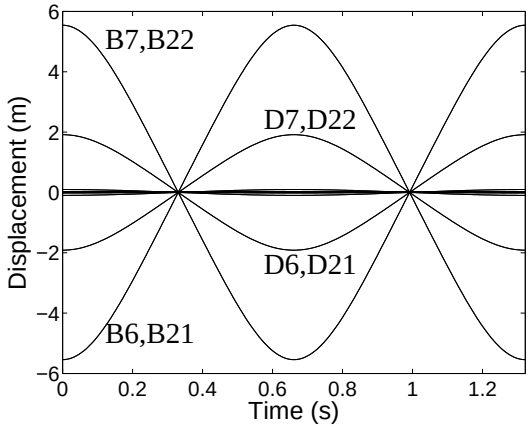

Figure 9: Time series corresponding to the localized NNM motion of mode (1,14) (see Figure 8).

coalesce into the backbone branch of another mode, thereby realizing an internal resonance between the two modes. For instance, Figure 10 depicts a 3:1 internal resonance between modes (0,6) and (1,12) in the FEP. To better understand the resonance mechanism, the backbone of mode (1,12) is represented at the third of its characteristic frequency (this is relevant, because a periodic solution of period T is also periodic with period $3T$). This demonstrates that a smooth transition from mode (0,6) to mode (1,12) occurs on the tongue. A further illustration is that motions M1 and M2, which are the motions right after and before the coalescence of the two NNM branches, are almost identical.

During this 3:1 internal resonance, the system vibrates along a subharmonic NNM; i.e., an NNM motion characterized by more than one dominant frequency component. On the branch of mode (0,6), the motion is characterized by one dominant frequency component, say ω. As we move along the tongue from this branch, a third harmonic progressively appears, and the system vibrates with two dominant frequency components ω and 3ω. As we progress further on the tongue, the third harmonic tends to dominate the component at the fundamental frequency, until this latter completely disappears. At this precise moment, a transition to mode (1,12) is realized. This transition is illustrated in Figure 11 using time series representative of the NNM motion at three different locations on the tongue.

Surprisingly, the ratio of the linear natural frequencies of modes (0,6) and (1,12) is far from 3; it is equal to 2.47. A 3:1 internal resonance between the two modes can still be realized, because the frequency of mode (0,6) increases much less rapidly than that of mode (1,12), as shown in Figure 4. This clearly highlights

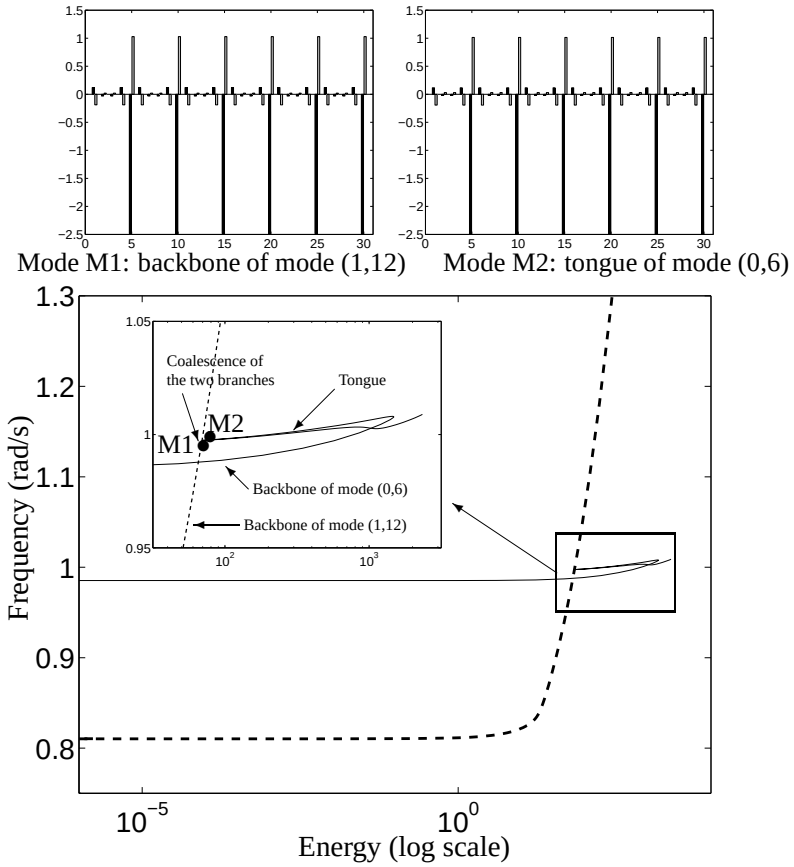

Figure 10: 3:1 internal resonance between modes of the mode pairs (0,6) and (1,12). The solid line corresponds to the backbone of one mode of the mode pair (0,6), which is continued by a tongue of internally resonant NNMs. The dashed line corresponds to the backbone of one mode of the mode pair (1,12) represented at the third of its dominant frequency.

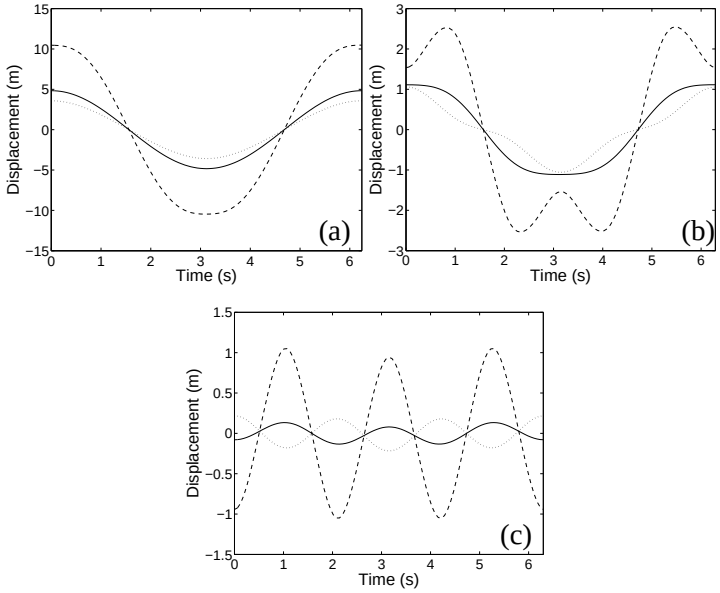

Figure 11: Time series corresponding to NNM motions on the tongue of 3:1 internal resonance (solid line: blade 1; dashed line: disk 10; dotted line: disk 14). (a) Beginning of the tongue (in the vicinity of the branch of mode (0,6)); (b) middle of the tongue; and (c) extremity of the tongue (in the vicinity of the branch of mode (1,12)).

that *NNMs can be internally resonant without necessarily having commensurate linear natural frequencies*, a feature that is rarely discussed in the literature. Another interesting finding is that *there is a countable infinity of branches of internally resonant NNMs in this system*, similar to what was reported for a 2DOF system in [3, 12].

By means of the sensitivity analysis, the computation of the branch depicted in Figure 10 requires 1 minute using a 2GHz processor. The finite-difference approach is computationally intensive and demands 15 minutes. Therefore, the sensitivity analysis significantly reduces the computational cost of the algorithm. This is an important feature when targeting a computationally tractable calculation of the NNMs. Due to the presence of turning points, the computation of the tongue in Figure 10 demands most of the CPU time.

Besides the NNMs described here, additional modes exist. In particular, NNM motions which take the form of traveling waves occur. They are represented by ellipses in the configuration space. A detailed analytical study of these modes is given in reference [20]. The examination of these additional modes is beyond the scope of this paper and will be addressed in subsequent studies [21].

5 Conclusion

In this paper, a numerical method for the computation of NNMs of mechanical structures was introduced. The approach targets the computation of the undamped modes of structures discretized by finite elements and relies on the continuation of periodic solutions. The procedure was demonstrated using a simplified discrete model of a nonlinear bladed disk, and the NNMs were computed accurately in a fairly automatic manner. Complicated NNM motions were also observed, including a countable infinity of internal resonances and strong motion localization.

This method represents a first step toward a practical NNM computation with limited implementation effort. However, two important issues must be addressed adequately to develop a robust method capable of dealing with large, three-dimensional structures:

- (i) Fundamental NNMs with no linear counterparts (i.e., those that are not the direct extension of the LNMs) have not been discussed herein. These additional NNMs bifurcate from other modes, and a robust branch switching strategy will be developed for their computation.
- (ii) The method relies on extensive numerical simulations and may be computationally intensive for large-scale finite element models. As a result, a further reduction of the computational cost is the next objective. To this end, a significant improvement was to use sensitivity analysis to obtain the Jacobian matrix as a by-product of the time integration of the current motion. An automatic time step control, which selects the most appropriate time step in view of the current dynamics, will also be considered to speed up the computations.

References

[1] A.F. Vakakis, L.I. Manevitch, Y.V. Mikhlin, V.N. Pilipchuk, A.A. Zevin, *Normal Modes and Localization in Nonlinear Systems*, John Wiley & Sons, New York (1996).

[2] A.F. Vakakis, *Non-linear normal modes (NNMs) and their applications in vibration theory: An overview*, Mechanical Systems and Signal Processing, Vol. 11, No. 1 (1997), pp. 3-22.

[3] G. Kerschen, M. Peeters, J.C. Golinval, A.F. Vakakis, *Nonlinear normal modes, Part I: A useful framework for the structural dynamicist*, Mechanical Systems and Signal Processing, in press (2008).

[4] J.C. Slater, *A numerical method for determining nonlinear normal modes*, Nonlinear Dynamics, Vol. 10, No. 1 (1996), pp. 19-30.

[5] E. Pesheck, *Reduced-order modeling of nonlinear structural systems using nonlinear normal modes and invariant manifolds*, PhD Thesis, University of Michigan, Ann Arbor (2000).

[6] Y.S. Lee, G. Kerschen, A.F. Vakakis, P.N. Panagopoulos, L.A. Bergman, D.M. McFarland, *Complicated dynamics of a linear oscillator with a light, essentially nonlinear attachment*, Physica D-Nonlinear Phenomena, Vol. 204, No. 1-2 (2005), pp. 41-69.

[7] R. Arquier, S. Bellizzi, R. Bouc, B. Cochelin, *Two methods for the computation of nonlinear modes of vibrating systems at large amplitudes*, Computers & Structures, Vol. 84, No. 24-25 (2006), pp. 1565-1576.

[8] R. Seydel, *Practical Bifurcation and Stability Analysis, from Equilibirum to Chaos*, Springer-Verlag, 2nd Edition (1994).

[9] A.H. Nayfeh, B. Balachandran, *Applied Nonlinear Dynamics: Analytical, Computational, and Experimental Methods*, Wiley-Interscience, New York (1995).

[10] E. Doedel, *AUTO, Software for Continuation and Bifurcation Problems in Ordinary Differential Equations*, (2007).

[11] C. Touzé, A. Amabili, O. Thomas, *Reduced-order models for large-amplitude vibrations of shells including in-plane inertia*, In *Proceedings of the EUROMECH Colloquium on Geometrically Nonlinear Vibrations, Porto, Portugal, July 2007*, Porto (2007).

[12] M. Peeters, R. Viguié, G. Sérandour, G. Kerschen, J.C. Golinval, *Nonlinear normal modes, Part II: Toward a practical computation using numerical continuation techniques*, Mechanical Systems and Signal Processing, in press (2008).

[13] O. Brüls, P. Eberhard, *Sensitivity analysis for dynamic mechanical systems with finite rotations*, International Journal for Numerical Methods in Engineering, Vol. 1 (2006), pp. 1-29.

[14] D.J. Ewins, *Structural Dynamics Characteristics of Bladed Assemblies*, Lecture Series 1992-06 on Vibration and Rotor Dynamics, Von Karman Institute for Fluid Dynamics (1992).

[15] R.M. Rosenberg, *On nonlinear vibrations of systems with many degrees of freedom*, Advances in Applied Mechanics, Vol. 9 (1966), pp. 155-242.

[16] M.P. Castanier, C. Pierre, *Modeling and analysis of mistuned bladed disk vibration: Status and emerging directions*, Journal of Propulsion and Power, Vol. 22, No. 2 (2006), pp. 384-396.

[17] A.F. Vakakis, C. Cetinkaya, *Mode localization in a class of multidegree-of-freedom nonlinear-systems with cyclic symmetry*, SIAM Journal on Applied Mathematics, Vol. 53, No. 1 (1993), pp. 265-282.

[18] A.F. Vakakis, T. Nayfeh, M.E. King, *A multiple-scales analysis of nonlinear, localized modes in a cyclic periodic system*, Journal of Applied Mechanics-Transactions of the Asme, Vol. 60, No. 2 (1993), pp. 388-397.

[19] M.E. King, A.F. Vakakis, *A very complicated structure of resonances in a nonlinear-system with cyclic symmetry: Nonlinear forced localization*, Nonlinear Dynamics, Vol. 7, No. 1 (1995), pp. 85-104.

[20] A.F. Vakakis, *Dynamics of a nonlinear periodic structure with cyclic symmetry*, Acta Mechanica, Vol. 95 (1992), pp. 197-226.

[21] F. Georgiades, M. Peeters, G. Kerschen, J.C. Golinval, M. Ruzzene, *Modal analysis of a nonlinear periodic structure with cyclic symmetry*, AIAA Journal, in preparation.